SPIRAL SECTOR FFAG MAGNET DESIGN AND FIELD MEASUREMENTS*

S. C. Snowdon, R. S. Christian, G. del Castillo, R. W. Fast
Midwestern Universities Research Association, USA
(Presented by S. C. SNOWDON)

A scaling spiral sector FFAG magnet has a magnetic field theat may be derived from the following magnetostatic potential

$$V=\left(\frac{r}{r_0}\right)^{k+1} F\left(\frac{1}{W}\ln\frac{r}{r_0}-N\theta,\ \frac{z}{r}\right),$$

where k is the field index, N is the sector number, r_0 is any convenient radius such as the average equilibrium orbit radius at full energy, and w is a measure of the pitch of the spiral [1]. The function F is periodic in its first variable, $\frac{1}{w}\ln\frac{r}{r_0}-N\theta$. In the infinite permeability approximation, this scaling magnetic field may be realized by a sequence of spirals of iron that are alternately energized (plus poles) and neutral (zero poles), the surface of the iron being situated on cones of constant z/r. The plus poles, however, must possess a surface potential that varies as $(r/r_0)^{k+1}$ along any spiral, a condition that is normally obtained by providing an excitation winding differentially graded through small radial slots in the plus pole.

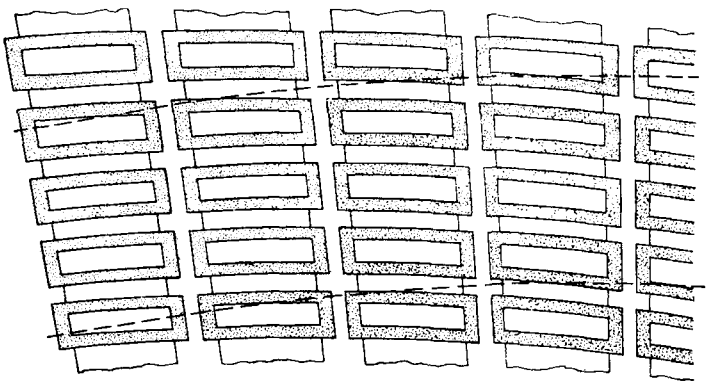

Fig. 1. Integral scaling pole face.

Any practical realization of a reasonably large spiral sector magnet must incorporate radial cuts (short straight sections) to modularize the magnet into manageable units. Fig. 1 indicates the nature of the approximation to the scaling field, which, since the scaling property obtains only for finite transformations, is termed integral scaling. The potentials of the plus poles are adjusted to give an r^{k+1} variation along each spiral ridge as one proceeds outward along the magnet blocks. A calculation of the particle motion in magnetic fields possessing integral scaling symmetry indicates that the deviation from scaling symmetry is acceptable so long as the straight sections are short and the number of radial cuts in relation to the number of sectors is made sufficiently large [2]. For instance, if 25% of the circumference is removed by radial cuts and there are nine magnet blocks for every two spiral sectors, the change in tune is less than 0.07.

Integral scaling symmetry has the property that the entire magnetic field may be found from the field existing in one cell by a simple multiplicative transformation. The ratio of fields at homologous points in any two cells is determined by the ratio of r^k to the centers of each of the two cells. Fig. 2 shows an enlargement of the unit cell consisting of a plus pole around which is placed an excitation coil. The choice of cell boundaries is flexible so long as it is the same for all cells. We take a cell to consist of half of a zero pole and half of the radial cut on each side of the plus pole. The cell includes, in the vertical direction, the space between the median plane up to a distance sufficient to outline all of the important features of the magnet such as the coil slots.

The magnetostatic problem of finding fields produced by distributed currents is formulated

* Supported by the U. S. Atomic Energy Commission.

in terms of a scalar function. In fact, the method employed constitutes a generalization of Ampere's method of solving magnetostatic problems [3]. The notion, familiar in the decomposition of electromagnetic fields into transverse electric and transverse magnetic

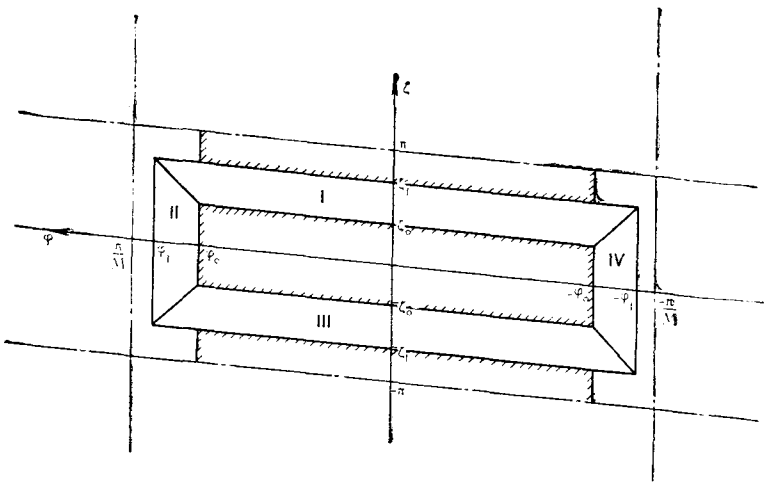

Fig. 2. Pole face unit cell.

waves [4], is employed to decompose the current density vector

$$\vec{J} = \vec{L}\sigma + \nabla \times \vec{L}\tau,$$

where, in the cases of interest,

$$\vec{L} = \vec{a} \times \nabla \quad (\vec{a} = \text{constant vector}).$$

For magnetic fields associated with circular accelerators, the vector $\vec{a}$ is chosen most conveniently to be a unit vector along the vertical or z-axis. In general, the determination of the scalar densities σ and τ that suitably represent $\vec{J}$ is a relatively simple matter since the spatial variation of $\vec{J}$ usually is not complex. Given the densities σ and τ, Ampere's circuital relation insures that the magnetic field may be represented by

$$\vec{H} = 4\pi\vec{L}\tau - 4\pi\sigma\vec{a} - \nabla V,$$

where the potential function is determined by the condition, $\nabla \cdot \mu\vec{H} = 0$, or, as is more convenient, its integral equivalent:

$$\oint \mu\,(4\pi\vec{L}\tau - 4\pi\sigma\vec{a} - \nabla V)\cdot\vec{ds} = 0.$$

Since σ and τ are presumed known, having been determined in such a way as to represent the current density, the above relation provides an integral equation for the determination of the potential V. For the case of iron with infinite permeability, the magnetic field is calculated only within the air and conductor region. The integral equation applied to the surface surrounding any point in a mesh of points constructed to represent the region of interest, provides a means of obtaining a finite difference equation with which the potential V may be found by iterative techniques.

For the magnet to be considered, a solution of the three-dimensional potential problem in the unit cell is carried out on a basic mesh of 80 radial units, 96 azimuthal units, and 40 units in height giving a total of 83,000 mesh points. The potential information at these points is handled in an IBM-704 computer by storing three adjacent radial planes of $80 \times 3 \times 40 = 9600$ mesh points in the core, the other planes remaining on call in the tape-handling units. An improvement in the initial guess for the potential distribution on the middle plane is effected by the application of the finite difference equation which relates the potential at the center point to a weighted sum of the potentials at neighboring points. This improvement is first iterated systematically throughout the center plane. The leading edge plane is returned to the tape and a new trailing edge plane brought in from the tape, thereby advancing the previous trailing edge to the center where its potential is systematically improved in the manner just described. This scanning process is repeated in a cyclical fashion until the change in potential distribution in one scan averaged over the mesh is less than some preassigned value. The process converges to a definite distribution by virtue of assigned boundary values for the potential on the iron and known source corrections to the finite difference equation within the distributed currents.

The fields so calculated are not only useful for particle orbit studies but in further design of the magnet. It will be noted that, as one proceeds outward along the spiral ridges,

a point is reached where the flux density in the plus pole attains a high saturation level. This can be eased if one changes the

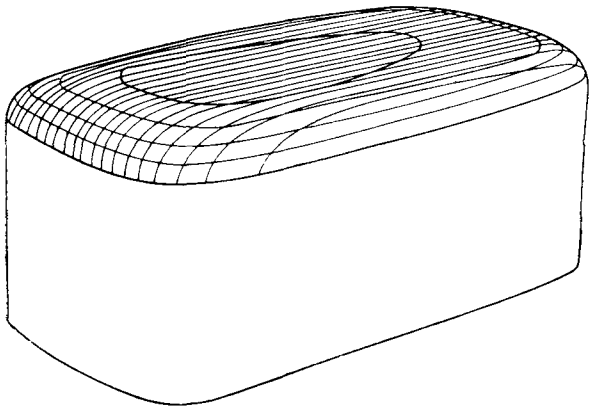

Fig. 3. Nonscaling pole.

pole shape to one that is determined by any one of the magnetostatic equipotentials. In so doing, fewer ampere turns are needed to excite the pole. Fig. 3 shows how the points on the equipotential surface are arranged into contours. These lines are of two types, curves of constant height or J-cuts, and curves in the spiral surface or I-cuts.

The next step is to erect a normal to this magnetic equipotential and is accomplished by calculating the magnetic field. A surface one inch away from the desired surface out along the normal is constructed and organized into the same I and J cuts. This is the surface that must be traversed by the center of a ball milling cutter. Point-by-point information for moving the center of a ball mill over the various contours was placed on punched tape to give machining instructions to a numerically controlled milling machine. In total about 3 500 instructions were required for each pole.

Fig. 4 shows two magnet blocks whose fields have been computed as described and whose outer poles have been shaped by contour milling. The various poles of the magnet may be seen together with the excitation coils, the return flux yoke, and the back leg. Fig. 5 shows a more recent view of the same two

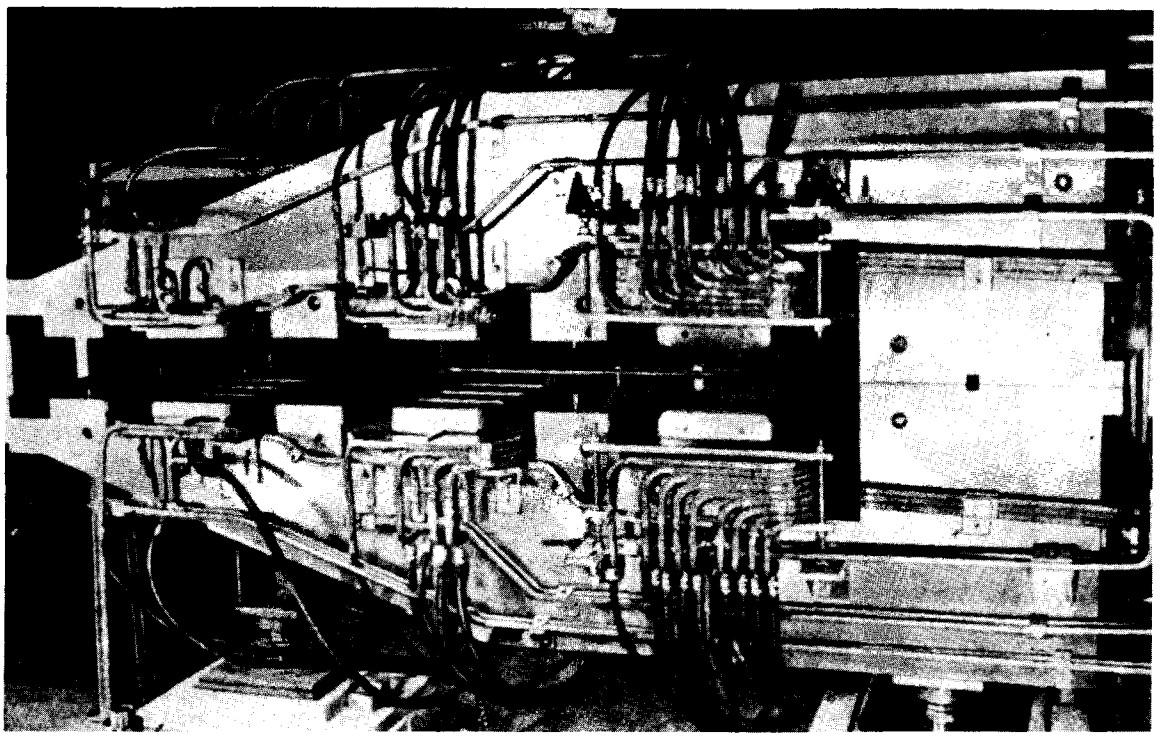

Fig. 4. Spiral sector magnet model — during assembly.

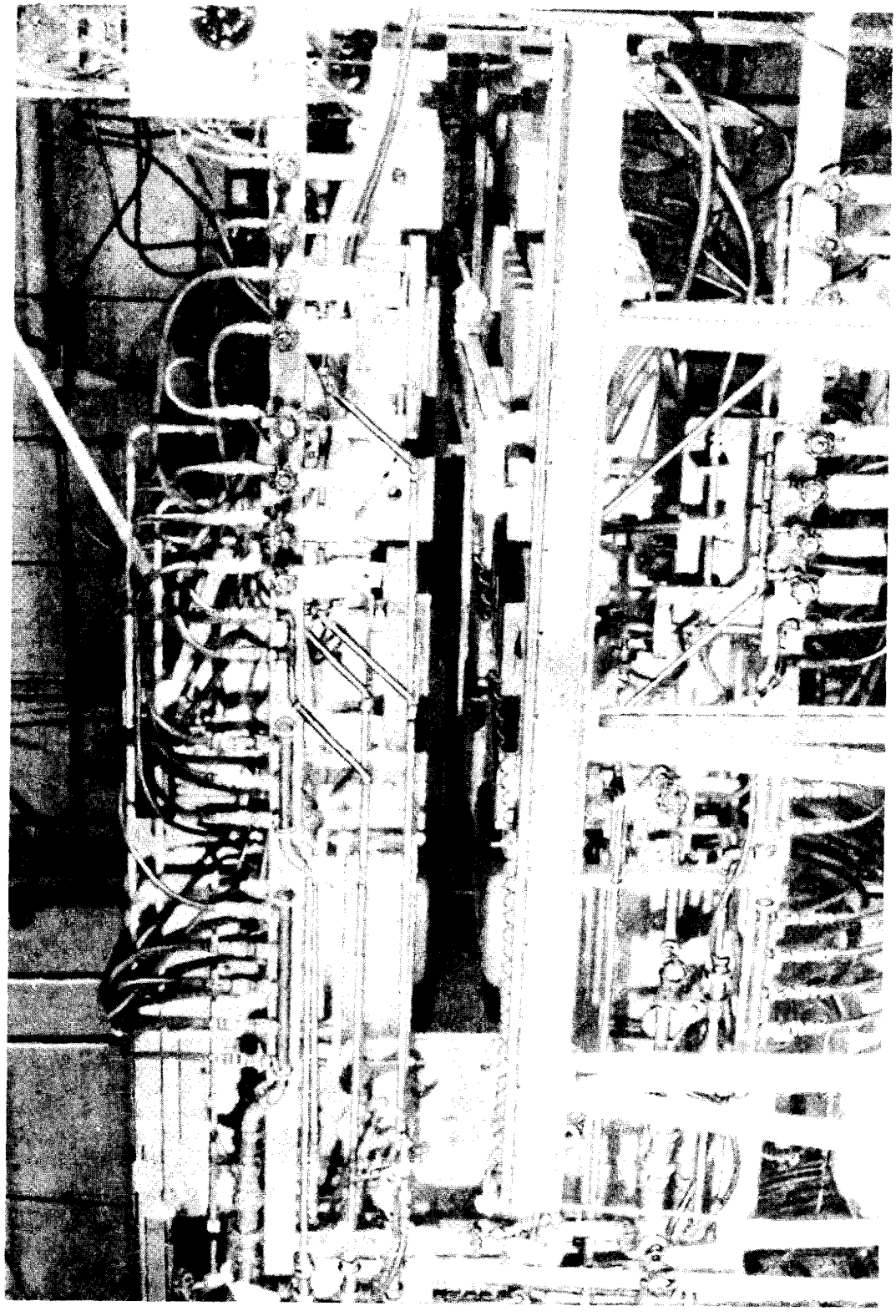

Fig. 5. Completed spiral sector magnet model with field measuring equipment in place.

magnets after the magnetic field measuring apparatus was added. The vertical field on the median plane was measured using a rotating coil-slip-ring assembly so designed as to reduce to negligible proportions all frequencies except the fundamental. This voltage was fed into an ac-dc converter and subsequently into a digital voltmeter. The system measures magnetic fields in the range of interest to a few parts in ten thousand.

In order to determine the proper excitations for each pole of the magnet, it is necessary to account for the reluctance drops in the iron and add these to the theoretical predictions for ideal iron. Although, in the experimental magnet under study, these excitations may be found empirically, it is desirable to be able to predict the reluctance drops in order to complete the theoretical design of the magnet. Two paths were followed in accounting for the properties of real iron, both of which attempted to account for the magnetic properties of real iron through the use of the normal induction curve. First, a semi-empirical approach through the use of a network of nonlinear magnetic circuits was employed to determine the potential of the positive and zero poles. The input information made use of air gap reluctances as determined from three-dimensional field computations for ideal iron and reluctance estimates of each iron segment from its area, length, and permeability. The permeability considered was an empirical function of the magnetic field.

With an assumed normal induction curve appropriate to low carbon steel, the 15-loop nonlinear curcuit, whose elements constitute the various air gap and iron segment reluctances, is solved by an iterative process. The loop fluxes were found for a convenient set of coil excitations that were present on the magnet. From these loop fluxes the median plane magnetic fields under the centers of the plus poles and zero poles were calculated. Solutions were obtained for twenty excitation situations ranging from low excitation to high excitation. The circuit theory calculations were compared with the measured fields and slight adjustments made in the assumed B (H) curve until a reasonable agreement with the measured values was obtained. The results for the plus poles are shown in Fig. 6, where the overall agreement is seen to be good to a few percent out of about a 30 percent deviation from the ideal iron case. Similar results shown in Fig. 7 were obtained for the zero poles where the trend of the measurements is clearly seen to be given by the circuit theory calculations.

The second path followed in tracing the effects of the magnetic flux flowing through iron was to solve the equivalent two-dimensional magnetostatic problem neglecting temporarily the fringing flux end effects. First,

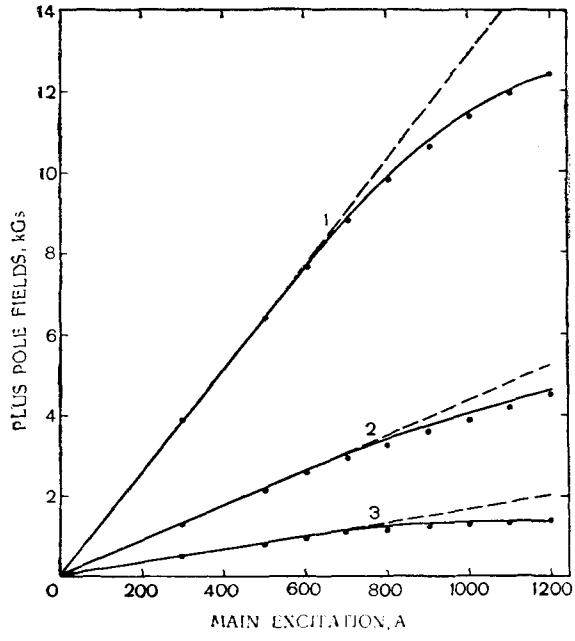

Fig. 6. Plus pole excitation curves. Excitation of magnet block A. (Theory — curves, experiment — points):

1 — nonscaling pole 53 turns; *2* — second plus pole 24 turns; *3* — third plus pole 8 turns, buckleg 3 turns.

the fields are found in the air assuming infinite permeability for the iron by the methods outlined previously. Next, the vector potential is found from this solution and, in particular, the values of this potential along the iron are used as boundary values for the solution of a vector potential problem within the iron. Since iterative methods are used throughout, it is possible to use the measured normal induction curve to insert the actual permeability at every point. The only approximation consists in assigning a constant vector potential to the outside edge of the iron thereby preventing any leakage of flux from the iron and incidentally fixing the net flux in the iron. The discontinuity in the magnetic scalar potential at the iron-air boundary within the magnet then serves to determine what surface distribution of currents ought to be placed

on the iron to have the real magnet yield the fields in the air as calculated with ideal iron boundaries. Of course, these surface currents are customarily approximated by distributing reluctance correction coils in as many points as is convenient, the total ampere turns involved being equal to the total required by the surface currents.

mates. In addition, however, it is possible to visualize the excessive potential gradients at the base of the shaped pole, a feature which will be employed to effect a redesign of the pole.

Given the fair agreement between the circuit theory predictions and the measured fields at selected points, it is a relatively simple calculational matter to determine a set of coil

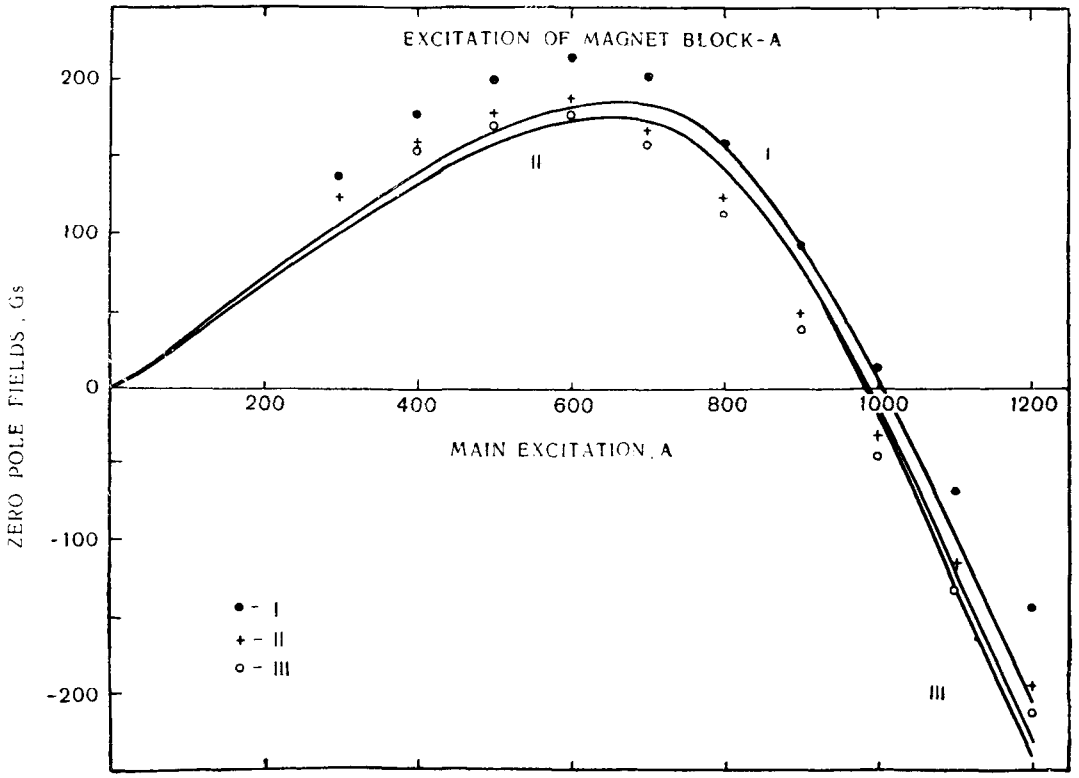

Fig. 7. Zero pole excitation curves. Excitation of magnet block A. (Theory — curves, experiment — points):
I — first zero pole; II — second zero pole; III — third zero pole.

Fig. 8 shows the result of this type of calculation as applied to a region of the magnet near the back leg. The shaped pole has been approximated by a beveled pole. In order to represent the flux flow in the actual magnet, the azimuthally fringing flux is accounted for approximately by seeking the vector potential distribution that yields a 14% higher maximum field, 14% being the percentage fringing flux involved as determined by comparing the flux from the three-dimensional calculation with flux per unit length from the two-dimensional calculation times the magnet width. The potential drops in the iron agree favorably with the circuit theory esti-

excitations that will yield the fields desired by the r^k scaling property. With the fields set at the correct values under the centers of each pole, a radial field map was taken and compared with the detailed computer fields. This is shown in Fig. 9. Fig. 10 shows a similar set of measurements taken in a transverse run across the plus poles and the radial gap.

The nature of the discrepancy between the measured and calculated fields in the radial run is shown in Figs. 11 and 12 for *A* and *B* magnet blocks at 100% excitation (12.5 kg at center of plus pole in *A* magnet). Figs. 13 and 14 show the same comparison at 50% excitation. When the 50% excitation runs were made, it was not

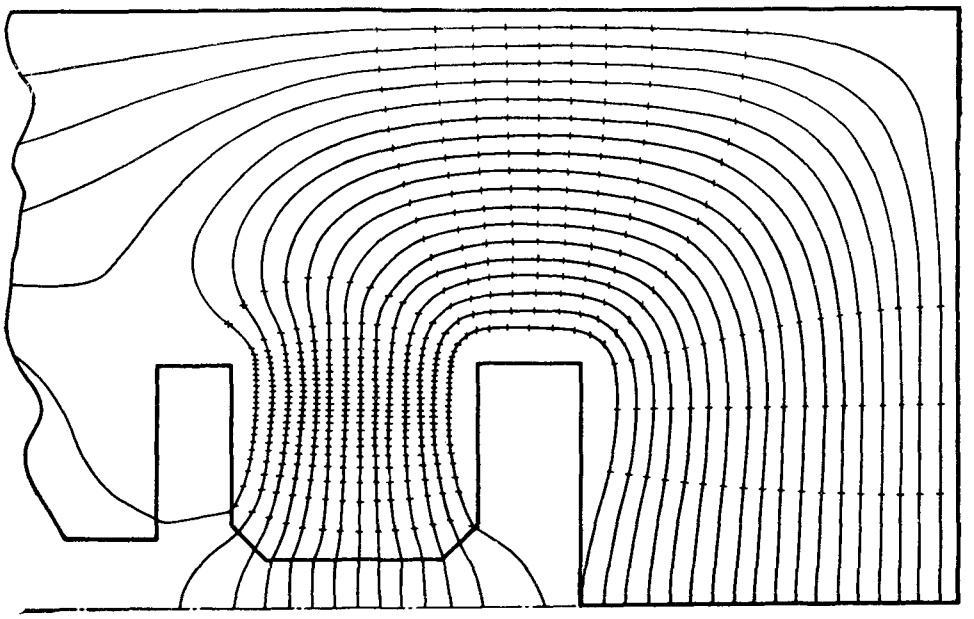

Fig. 8. Flux flow in nonscaling pole region.

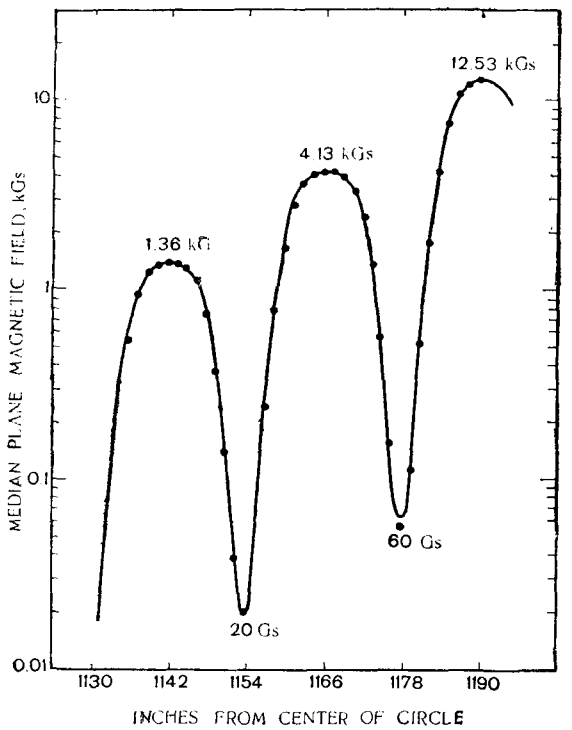

Fig. 9. Radial variation of median plane magnetic field. (Theory — curve, experiment — points).

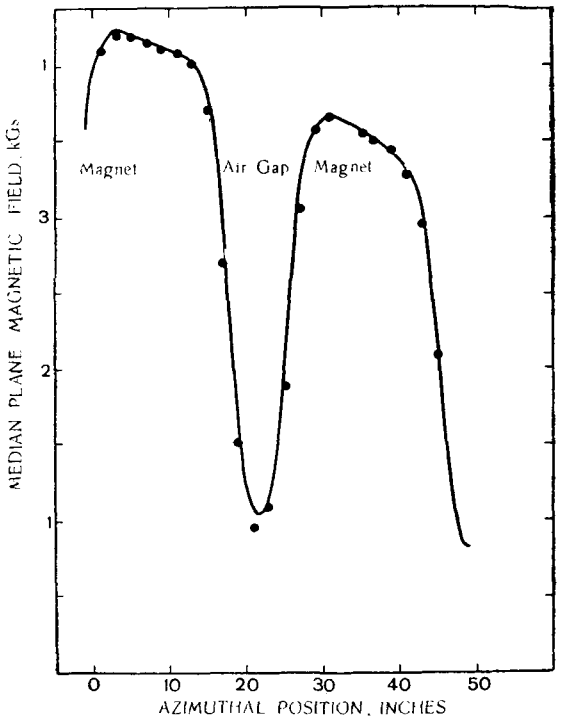

Fig. 10. Azimuthal variation of median plane magnetic field (Theory — curve, experiment — points).

expedient to neutralize the zero poles; and similarly when the 100% excitation runs were made, the innermost zero pole was not neutralized. These conditions plus the variation of the zero pole potential predicted by the magnetic circuit account completely for the variation and sign of the zero pole fields shown in Figs. 11—14. Since the change of r^k from the center of a plus pole in magnet B to the center of the corresponding pole in magnet A is only 13% the radial runs in magnets A and B give essentially identical effects for any given excitation.

The observations then are that for a fixed excitation the discrepancy in the neighborhood

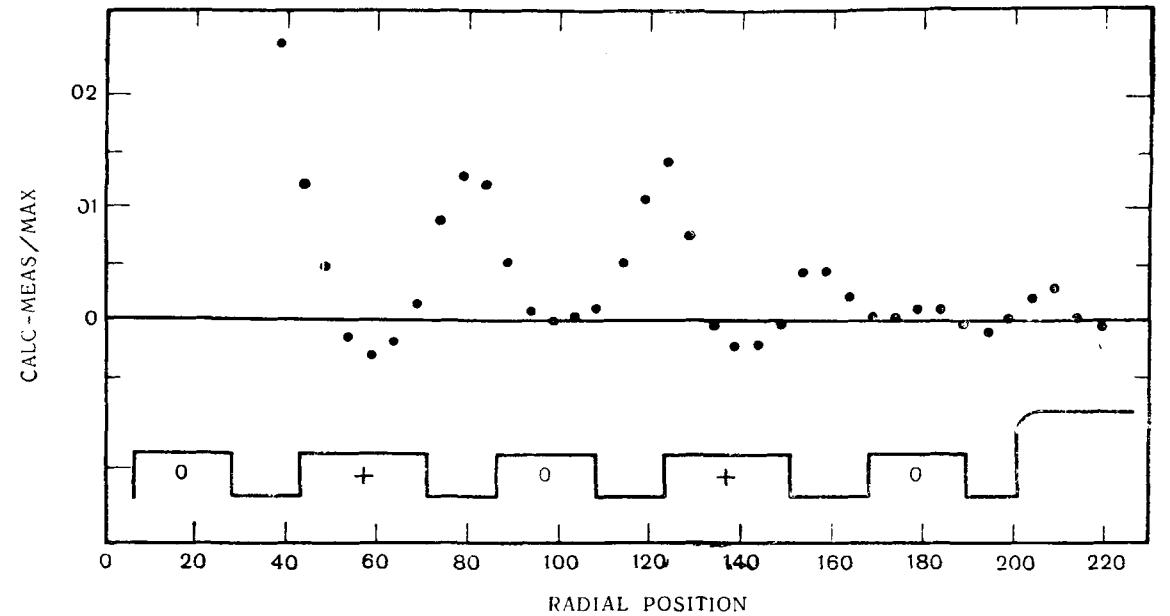

Fig. 11. Comparison with calculated fields, radial run, 100% excitation, middle of a magnet A.

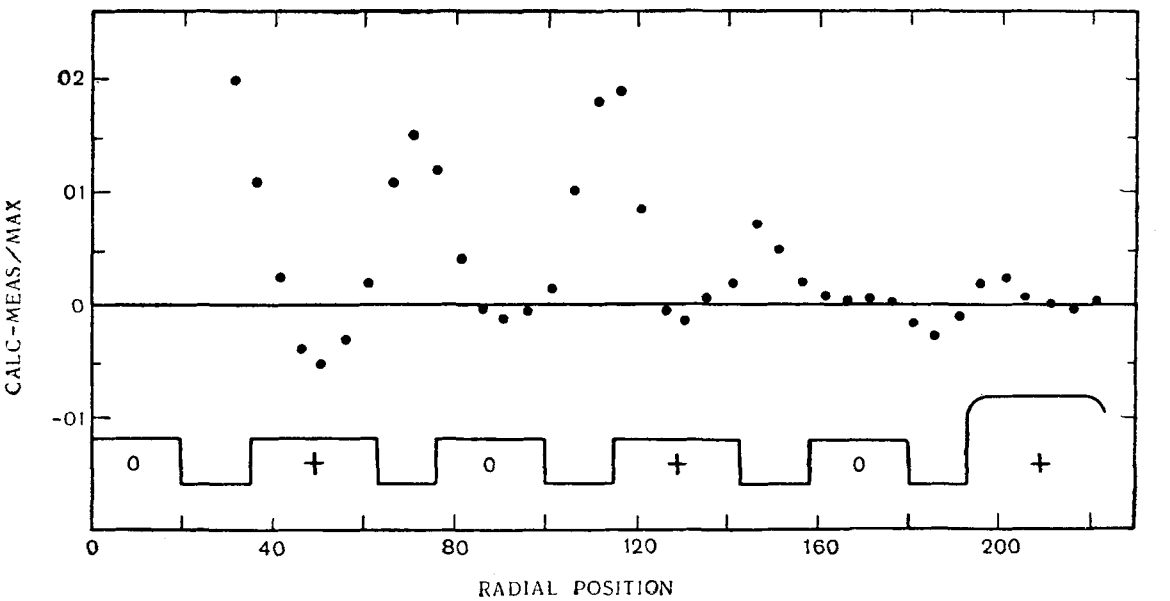

Fig. 12. Comparison with calculated fields, radial run, 100% excitation, middle of a magnet B.

of the scaling poles is larger than in the shaped or nonscaling pole. As the excitation is increased from 50 to 100%, the variation of the discrepancy with radius becomes somewhat larger. It is, however, not proportional to the excitation. The general conclusion from the scaling features between cells such as different current slot depths. In making comparisons between calculations and measurements, a nonscaling pole cell calculation was available together with a scaling pole cell calculation appropriate to the middle plus pole situation. The

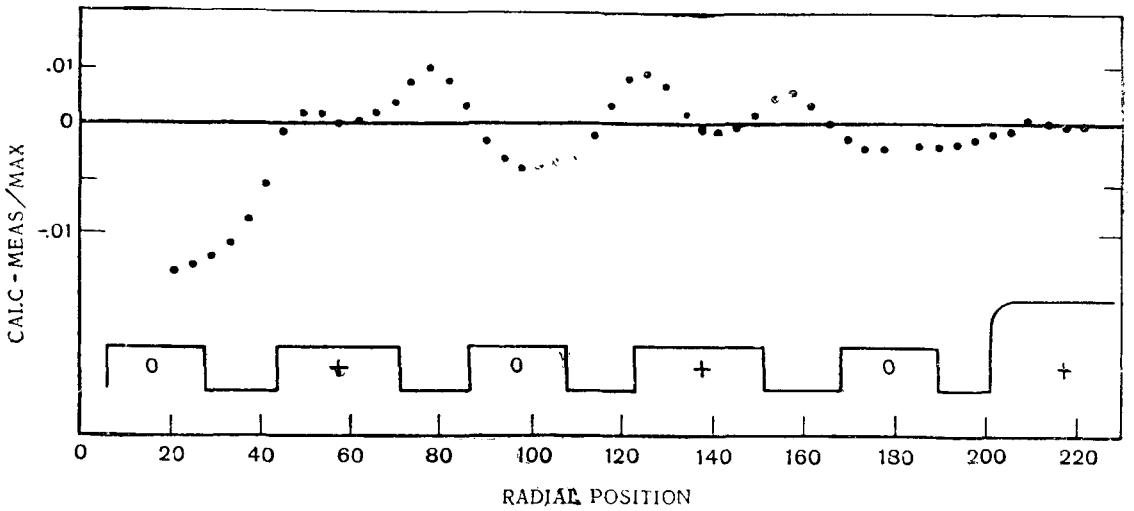

Fig. 13. Comparison with calculated fields, radial run, 50% excitation, middle of a magnet A.

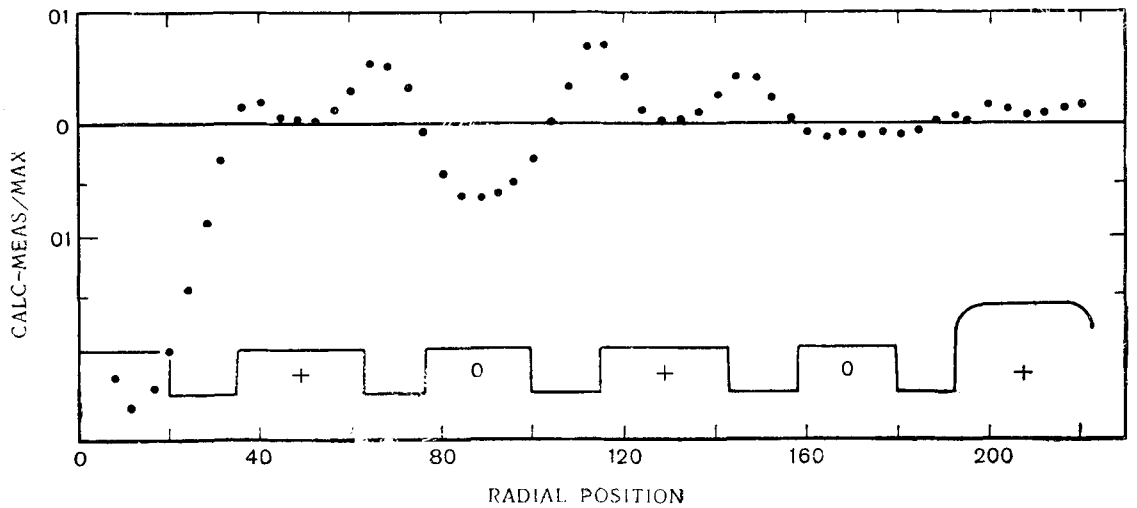

Fig. 14. Comparison with calculated fields, radial run, 50% excitation, middle of a magnet B.

radial runs is that the deviation of the calculation from the measurement follows a smooth pattern whose maximum is 1.5%.

Because the zero poles effectively shield one cell from its radially adjacent cell, if separate calculations are available for each cell, they are accurate within 0.1% regardless of non-innermost cell comparison was made using the fields of the middle cell suitably adjusted to yield the innermost pole field at the center of the plus pole. Since the actual slots for this cell are less deep than those for the middle cell, the measured fields are smaller on this account. It is to be expected, therefore, that

the percentage discrepancy for both scaling cells would be the same if this nonscaling change in slot depth were accounted for.

The remaining discrepancy of about 1% may be accounted for by some feature of the magnet structure such as the finite width of the potential grading slots, that was not taken into account in the calculation. Preliminary estimates indicate that this feature can explain the effect. Furthermore, the finite potential grading slot effect was not present in the nonscaling pole where the agreement between calculations and measurement is best. Finally it is to be noted that, since there is very little difference in the variation of the discrepancy between 50 and 100% excitation, saturation on the edges of the scaling poles cannot be an important feature.

Figs. 15 and 16 show the discrepancy between the calculated and measured median plane fields in transverse runs across each of the plus poles and the intermediate two zero poles for 100% excitation. Again the discrepancies generally become smaller toward the nonscaling pole. These discrepancies are accounted for by the following arguments. The potential on the vertical surface of the iron yoke in the straight sections varies from a positive potential near the back leg where the main reluctance correction coil was placed to negative values as one proceeds to the innermost radius. The sign of all the discrepancies in Figs. 15 and 16 that are positive can be explained by the presence of a negative potential on the yoke surface. The zero pole discrepancy that is negative requires a positive potential on the yoke and hence one may assume that the change in sign from negative to positive occurs prior to reaching the zero pole adjacent to the nonscaling pole. This explanation requires that the nonscaling pole discrepancy be negative which it does not appear to be. It is to be noted, however, that the potential information used to construct

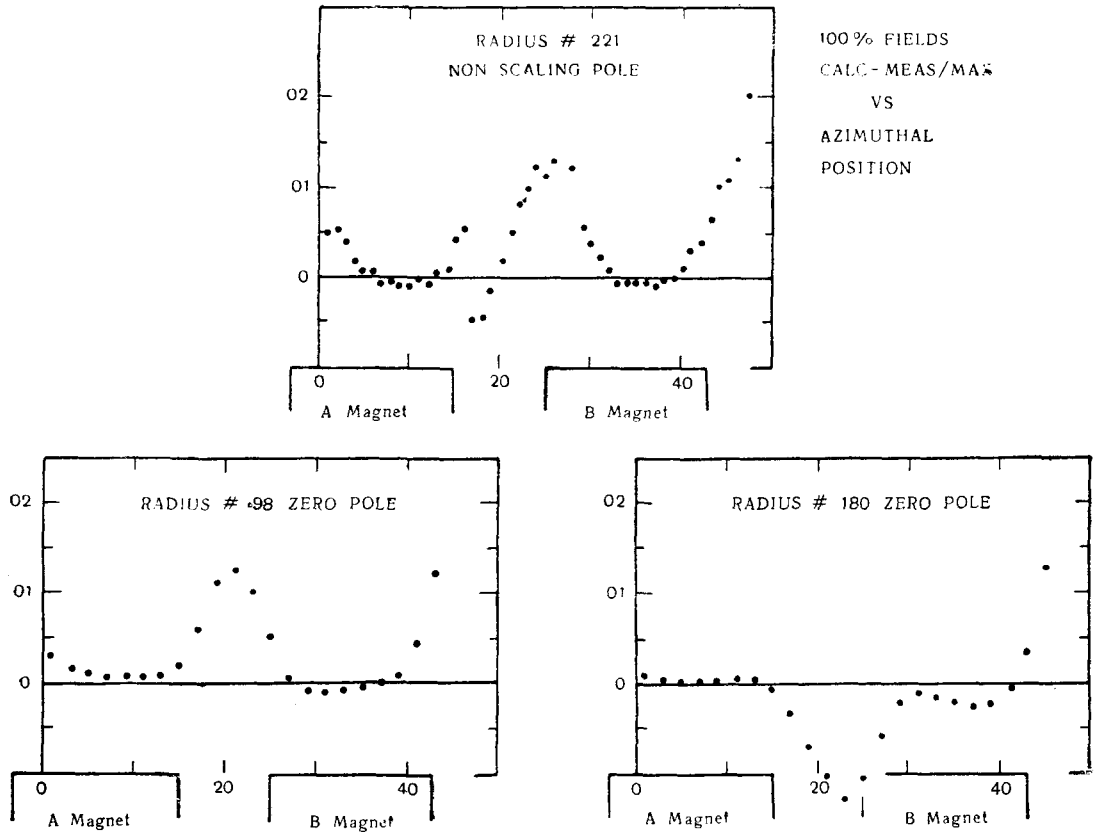

Fig. 15. Comparison with calculated fields, azimuthal runs, 100% excitation.

the equipotential surface of the nonscaling pole was obtained in an early stage of the calculation and actually was determined on too coarse a mesh in the azimuthal direction. This, together with the greater irregularity of the discrepancy with azimuth, makes it plausible to omit this pole run from the general argument.

further into the slots by 0.25 inches reduced the plus pole transverse run discrepancies to about 1%. This, again, may be explained by noting that this depression exposed more positive pole thus tending to cancel the effect of the negative potential below the coil. Furthermore, the radial run measurements

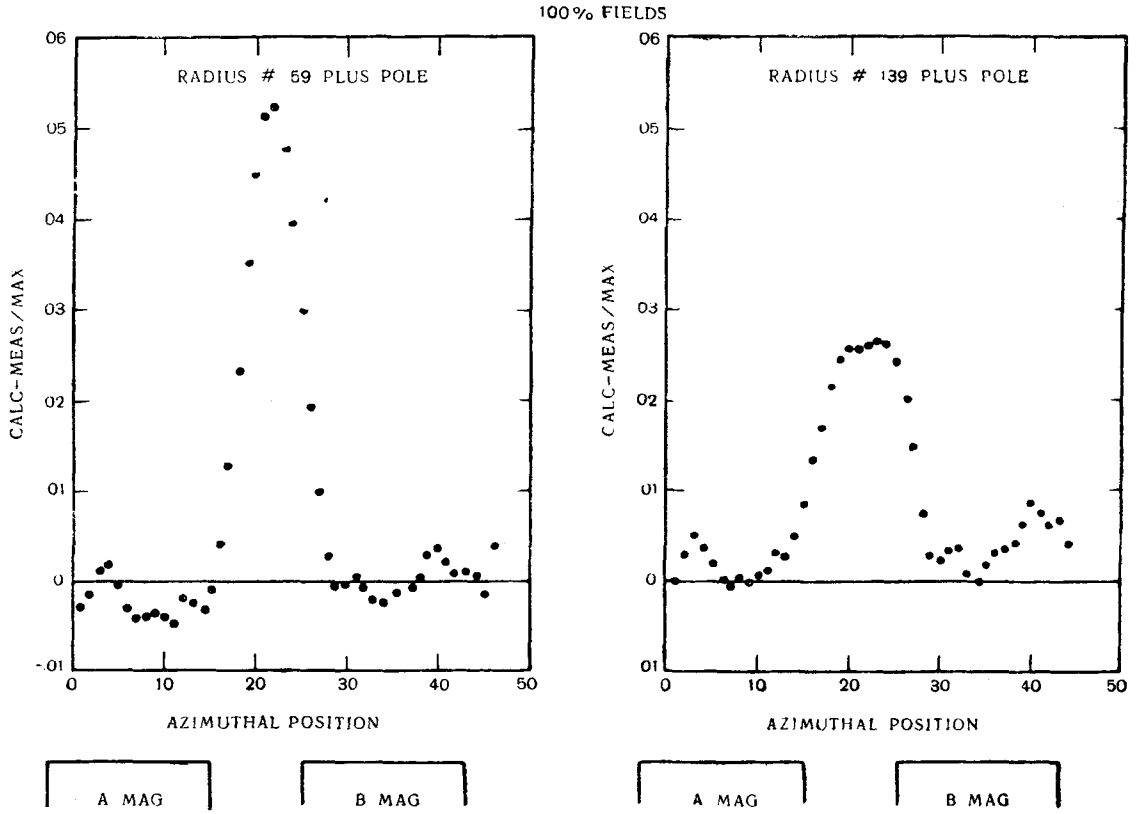

Fig. 16. Comparison with calculated fields azimuthal runs, 100% excitation (continued).

Two-dimensional estimates of the effect to be produced by a negative potential just below the coil indicate magnitudewise that a yoke potential about 1000 A turns can explain the observed discrepancies. Since this is just the order of ampere turns that were required to neutralize the zero poles, it seems quite reasonable to attribute all of the transverse run discrepancies to this effect. Of course, again the innermost pole measurements were compared with the middle pole calculations adjusted to give the correct fields as in the radial runs. This accounts for the unusually high discrepancy at this radius.

As an aid in removing these discrepancies, it was noted that moving the excitation coils were not changed by more than 0.2%, presumably because the zero pole is sufficiently close to the plus pole to receive the added flux instead of letting it pass through the median plane.

Fig. 17 shows the same plus pole transverse run discrepancies for 50 excitation. No runs were made across the zero poles since they were not neutralized. Again the discrepancy between calculated and measured fields improves as one moves toward the nonscaling pole and is generally understood by the previous arguments.

In conclusion, the measured median plane fields in a spiral sector FFAG magnet structure agree with the calculated fields to the

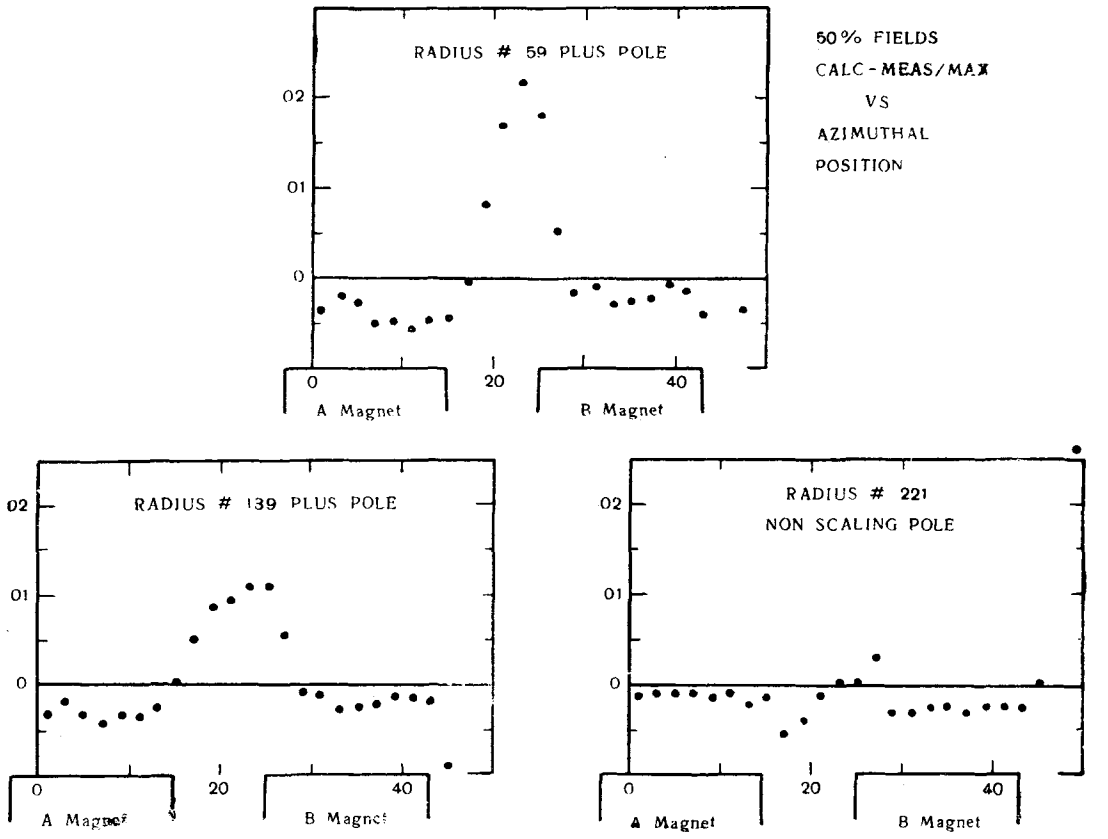

Fig. 17. Comparison with calculated fields, azimuthal runs, 50% excitation.

order of one percent. With small calculable adjustments of the coils this agreement may be of the order of 0.1%.

REFERENCES

1. Symon K. R., Kerst D. W., Jones L. W., Laslett L. J. and Terwilliger K. M. Phys. Rev., **103**, 1837 (1956).
2. Parzen G. Private communication.
3. Sommerfeld A. Electrodynamics, Academic Press, 1952, Part I, Section 16.
4. Stratton J. A. Electromagnetic Theory, McGraw-Hill Book Co., Inc., New York, 1941, Chapter VII.
   Smythe W. R. Static and Dynamic Electricity, McGraw-Hill Book Co., Inc., New York, 1950, Chapter VII; see also Snowdon S. C. J. Math. and Phys., **2**, 719 (1961); Livingston M. S. and Blewett J. P. Particle Accelerators, McGraw-Hill Book Co., Inc., New York, 1962, Chapter VIII.

DISCUSSION

A. P. Fateev

At one time, the MURA group presented two 10 GeV accelerator projects. Why was this particular spiral variant chosen?

S. C. Snowdon

This question should be referred to Dr. Waldman, Director of MURA.

B. Waldman

Originally MURA designed and proposed a colliding beam accelerator of the radial sector type. In 1960 our objective was changed to that of producing a high intensity accelerator with a single beam. At the 1961 International High Energy Accelerator Conference a proposal was presented for a 10 GeV FFAG High Intensity proton accelerator. This has been changed recently to 12.5 GeV

V. N. Kanunnikov

Is it possible to name the basic parameters of the 12.5 GeV accelerator taking into account the magnetic field and accuracy of the magnetic measurements?

S. C. Snowdon

I shall answer only with respect to the magnet parameters:

R. (EQU. ORB.) = 3488 inches
H_{max} (EQU. ORB.) = 12.5 Gs
K (field index) = 85
Tangent spiral angle with respect to circle = 48/54
Number of spiral sectors = 48
Number of magnet blocks = 264
$R_{inj.}$ = 3345.5 inches.

B. N. Yablokov

What is the injection energy and what type of injector is chosen for the 12.5 GeV accelerator?

S. C. Snowdon

The injection energy is 200 MeV and is to be obtained from a linac. Other questions relative to the injector should be referred to Dr. Young.

A. V. Crewe

What is the weight of the magnet of the MURA machine?

S. C. Snowdon

23.000 t approximately.